ARTICLE IN PRESS

Ceramics International xxx (xxxx) xxx

Contents lists available at ScienceDirect

Ceramics International

journal homepage: www.elsevier.com/locate/ceramint

Electromagnetic modeling of tunability of Barium Strontium Titanate and Magnesium Borate composites[☆]

Prannoy Agrawal [a,1,*], Stipo Matic [a], Kevin Häuser [b], Joachim R. Binder [b], Holger Maune [c], Ersin Polat [a], Rolf Jakoby [a,2]

[a] Institute of Microwave Engineering and Photonics, Technical University of Darmstadt, 64287 Darmstadt, Germany
[b] Institute for Applied Materials, Karlsruhe Institute of Technology, 76021 Karlsruhe, Germany
[c] Microwave and Communication Engineering, Otto von Guericke University Magdeburg, 39106 Magdeburg, Germany

ARTICLE INFO

Keywords:
EM modeling
Ferroelectric-composites
Barium Strontium Titanate (BST)
Composite tunability model
Magnesium Borate (MBO)

ABSTRACT

A complete tunability electromagnetic simulation model for the $Ba_{0.6}Sr_{0.4}TiO_3$ (BST), with $\varepsilon_r \approx 2000$, and $Mg_2B_2O_6$ (MBO), with $\varepsilon_r \approx 7$, composites is proposed here. The model is based on electrostatics, to simulate the effects of bias fields distribution in the composite varactor at the unbiased state to create the biased state for all volumetric mixture compositions. A bulk-ceramic varactor approach is chosen for the fabricated varactors. Varactors are fabricated with different volume compositions of BST and MBO, ranging from 10 to 100 vol-% of BST. Simulated results of the varactor model are then verified with the measured results of the varactor. The simulated and measured tunability shows considerable discrepancy at room temperature, which leads to Curie temperature T_C investigation of the fabricated varactors. It has been observed that a shift in T_C is directly proportional to the discrepancies in the simulated and measured tunability. After incorporating the T_C shifts in the model, the results show close proximity between measured and T_C-shifted simulated tunabilities with differences being reduced from around 32% to 2% for 80 vol-% BST varactor.

1. Introduction

Rapid increase in the modern wireless devices have pushed the minimum structure size to atomic scale boundaries and thus, the focus is on improving the manufacturing processes. The plasma-enhanced deposition or etching are mostly used in these process [1], where the plasma is generated using high-power radio frequency (RF) continuous-wave (CW) signals, located in the lower ISM-bands such as 13.56 MHz. To maintain a continuous and smooth operation between plasma chamber and RF power generator, an impedance matching circuit is used during the plasma ignition and operation intervals. Currently, these circuits are based on mechanically-tuned vacuum capacitors, which suffers from limited tuning response times of around 1 s for maximum tunability. The decreasing thickness of the processed layers leads to decrease in plasma process intervals, forcing the tuning response times to sub-second domain [2]. Consequently, few solutions based on semiconductor varactor diodes, PIN-diode switched-capacitor banks and microelectromechanical systems (MEMS) switches have been implemented. Despite their advantages, semiconductor varactor diodes offer low Q-factors, limited power handling and low linearity, and PIN-diode switched capacitor banks do not provide continuous tunability [3–5]. MEMS-based solutions have shown promising results, but under hot switching condition in plasma applications, they suffer from poor power handling and inconsistent mechanical performance [3,6,7].

Recently, high dielectric and non-linear ferroelectrics such as $Ba_xSr_{1-x}TiO_3$ (BST) have been potential candidate for tunable microwave devices such as varactors, phase shifters and tunable filters [8–11]. The main advantages of these materials are high capacitance tunability, low tuning response times (<1 s), small leakage current (<1 µA) and high breakdown field strength (>1 kV/mm region). However, the BST and other ferroelectrics deal with the high sinter temperatures (>1200 °C), posing design limitations, and low Q-factors Q_ε (<150) degrading the overall device performance, which leads to higher insertion loss. Apart from these drawbacks, $Q_\varepsilon = 1/tan(\delta_\varepsilon)$, being inversely proportional to the frequency, makes it difficult to use these materials at higher frequencies for high Q_ε applications. These challenges led to the need for lower-loss ferroelectric materials. One such method is to mix low relative permittivity ε_r and high Q_ε materials in the

☆ This document is the results of the research project funded by the Deutsche Forgemeineschaft (DFG) under the project BI 1636/2-3 and JA 921/37-3.
* Corresponding author.
E-mail addresses: prannoy.agrawal@tu-darmstadt.de (P. Agrawal), rolf.jakoby@tu-darmstadt.de (R. Jakoby).
1 Researcher.
2 Supervisor.

https://doi.org/10.1016/j.ceramint.2022.09.202
Received 27 July 2022; Received in revised form 12 September 2022; Accepted 16 September 2022
Available online 23 September 2022

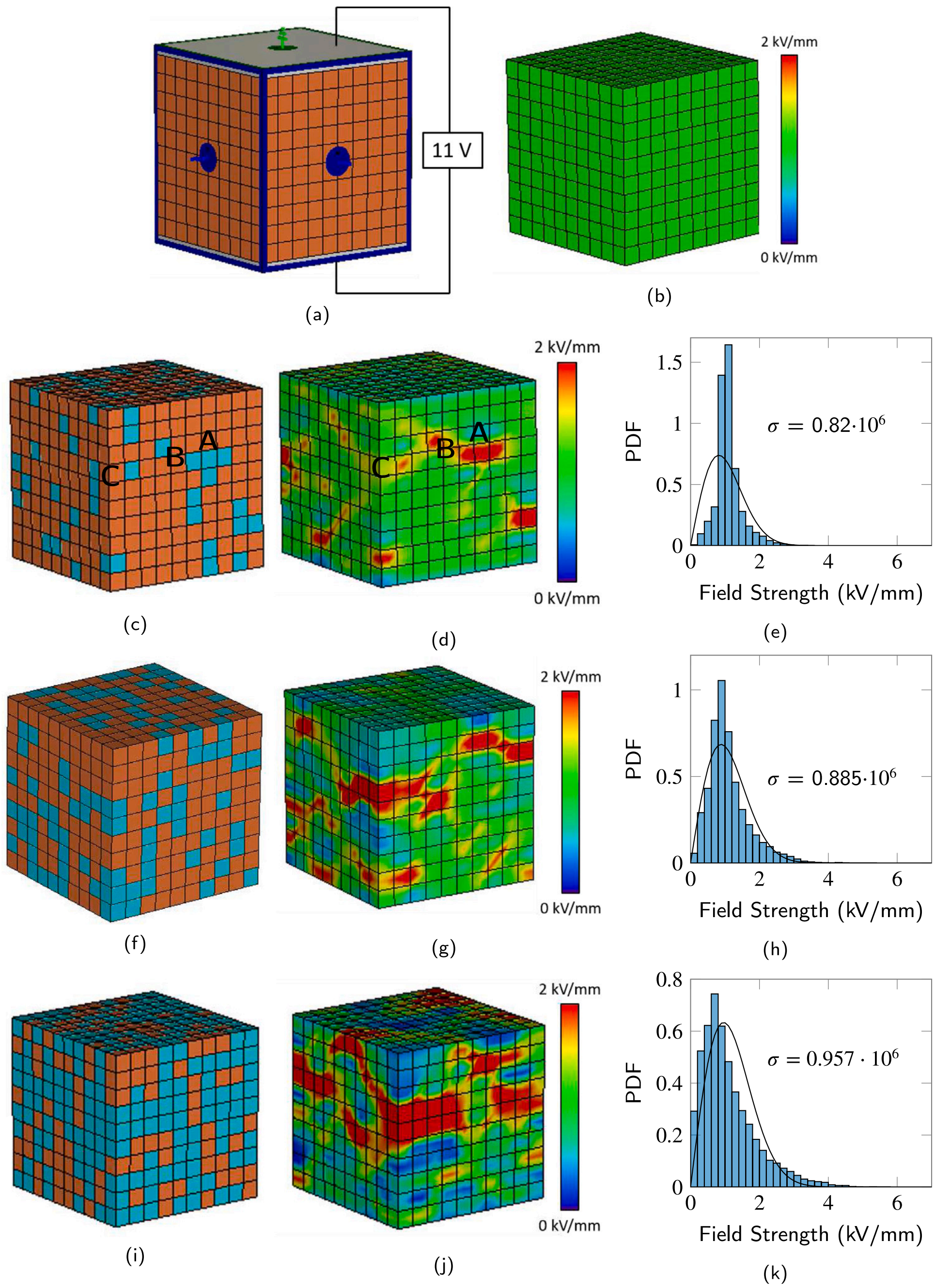

Fig. 1. Varactor model in CST Microwave Studio where (a), (c), (f), (i) represent the model in 100, 80, 60, 40 vol-% BST compositions, respectively, and (b), (d), (g), (j) show the flow of electric fields in the respective compositions. (a) also displays the set boundary conditions which are electrical boundaries at the top and bottom face, and magnetic boundaries at the other faces. An 11 V bias is applied between top and bottom face to generate electric fields of 1.1 kV/mm. (e), (h), (k) show the probability density function (PDF) of bias electric fields across the mesh cells in 80, 60, 40 vol-% BST compositions, respectively, with blue bars. The black line represents the Rayleigh distribution fit with σ being its Rayleigh parameter. (For interpretation of the references to color in this figure legend, the reader is referred to the web version of this article.)

pure ferroelectrics to reduce losses in ferroelectrics. Few additives have been showcased such as Magnesium Oxide (MgO) [12,13], Magnesium Silicate (Mg_2SiO_4) [14], Magnesium Titanate (Mg_2TiO_4) [15] and Magnesium Borate ($Mg_3B_2O_6$) [16]. The $Mg_3B_2O_6$ (MBO) has extremely high Q_ε (>2000) and is effective in reducing sinter temperatures and thus, is the optimum choice for this work [16].

Usually, these engineered composite materials have been investigated experimentally but precise modeling of these material's behavior is needed for better device design in the simulation environment. Few analytical and basic numerical models, as mentioned in [17,18], which are predicting the capacitive properties on the basis of a Bruggeman type of effective medium approximation (EMA) theory have been proposed. The main drawback is the inaccurate modeling or experimental deviation of tunability of the composites with all volume fractions of ferroelectrics. In parallel, Sherman et al. [19] produced a modified EMA (MEMA) model and its accuracy is limited to the very high vol-% of the ferroelectrics. Due to the advancements in the 3D electromagnetic simulation area, few computer-aided (CAD) models started flowing in, such as [20], which considers cubic phases for ferroelectric as well as dielectric, but showed a huge deviation from experiments. Another CAD model presented in [21] is close to the real structural scenario, considering properties such as varying sizes and overlapping of different ferroelectric phases. However, this model shows experimental

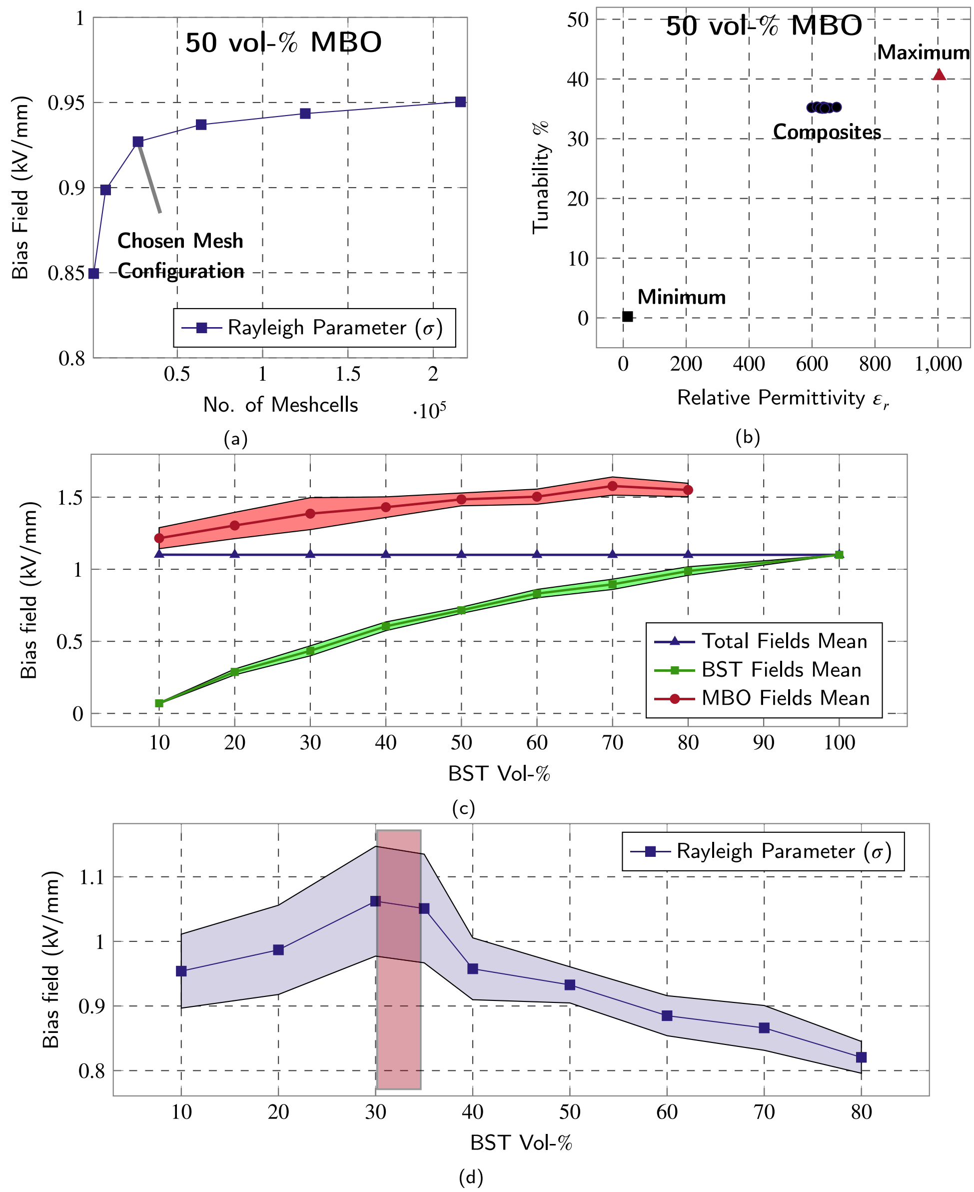

Fig. 2. (a) shows the selection criteria of no. of meshcells, in the 50 vol-% MBO composition, which starts converging after the chosen mesh configuration. The trade-off between accuracy and complexity is the main reason for this mesh selection. (b) demonstrates the variation of τ_ε with untuned ε_r of the 50 vol-% MBO composition. The black square and red triangle denote the extreme cases possible and blue dots denote the ε_r of different random arrangements of BST-MBO composites. The permittivity and τ_ε variation in the blue dots is around 6% and 0.25% from their respective mean values. (c) depicts average simulated bias fields extracted with shaded region demonstrating the variation with different random arrangements of BST and MBO. (d) shows the Rayleigh parameter σ of total electric field distribution with different vol-% of BST and MBO in the untuned varactor. The shaded region here again depicts the random arrangements variation. The σ first increases and then decreases around 30 vol-% BST indicated by a red box. This shift of electric field from the BST to MBO region denotes the percolation threshold limit. (For interpretation of the references to color in this figure legend, the reader is referred to the web version of this article.)

proximity with less than 60 vol-% of ferroelectrics. According to the author's knowledge, the main drawback faced by all these models is the limited consideration of the distribution of the electric fields inside the ferroelectric and dielectric under the influence of DC bias which is affecting the dielectric properties of the composites.

In this work, the aspect of tunability is focused upon and an efficient model for predicting tunabilities of the bulk-ceramic composite varactors for any composition of BST and MBO. The base design approach of the randomized cubical phase distribution of ferroelectric–dielectric materials, as discussed in [20,22], is considered which neglects the porosity effect (air gaps between different phases), shape and overlapping of different phases in the real mixtures. The objective of the model is to produce the effective electric field distribution to produce the tunabilities in accordance with the experiment analysis for all the volume compositions of BST-MBO mixtures.

2. Simulation methodology

A random-arranged cubic phase model is chosen for the simulation environment in the CST Studio Suite. This model includes 1000 cubes of 1×1 μm^2 divided among BST and MBO materials based on different volume compositions. The BST is taken to be as $Ba_{0.6}Sr_{0.4}TiO_3$, due to its Curie temperature around 0 °C to measure at room temperature [23]. The temperature difference ensures the BST operates in the paraelectric or non-polar phase to maintain centrosymmetry [23]. The BST has ε_r of around 2000 and Q_ε of around 100 in lower MHz range [21]. The MBO has a ε_r and Q_ε of around 7 and 2500 [21], respectively. These cubes are randomly placed to get a whole cube of 10×10 μ m^2, as shown in Fig. 1(b), for 100 vol-% BST composition. To create the effect of a parallel-plate capacitor, the whole cube is bounded by electric boundaries at the two opposite vertical faces which is denoted by gray

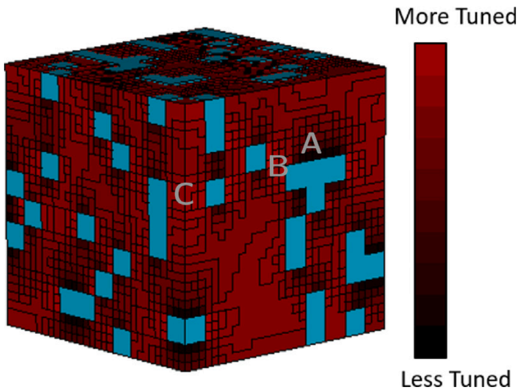

Fig. 3. Tuned varactor model for 80 vol-% BST depicting tuned model design with more redness indicating the extent of tuning. Point A represents the region with less bias electric field Fig. 1(e), so, less tuned BST in this region is depicted by dark red. Similarly, points B and C represent the high bias electric field regions, so, the more tuned BST in this region is shown by bright red. (For interpretation of the references to color in this figure legend, the reader is referred to the web version of this article.)

perfect electrical conducting (PEC) layer, depicted in Fig. 1(b). These boundaries are provided with a voltage potential difference of 11 V. A voltage difference or DC bias of 11 V corresponds to the 1.1 kV/mm of an overall electric field. The model varactor is surrounded by magnetic boundaries on the other faces to prevent the leakage of normal electric flux. The model varactor is simulated by using the Electrostatic Solver of CST, which results in the electric fields distribution and the capacitance of the model varactor in the non-biased state. The 3D bias electric field distribution indicates the extent of bias field flowing through each solid cube, as shown in Fig. 1(c), for the 100 vol-% BST composition varactor model. For 80 vol-% BST varactor model, shown in Fig. 1(d), the bias electric field distribution and their probability distribution function (PDF) is illustrated in Figs. 1(a) and 1(e). Similarly, Figs. 1(f)–1(h) depicts the model, bias fields distribution and their PDF for 60 vol-% BST varactor model, respectively. In addition, Figs. 1(i)–1(k) are for 40 vol-% varactor in the same order. The blue bar graph shows the PDF of the average bias electric field in each mesh cell across different cubes and the black line graph indicates the Rayleigh distribution fit of the same bias fields. This Rayleigh fit is characterized by the Rayleigh parameter σ, which estimates the behavior of the composite varactor. The increasing σ with increasing MBO vol-%, denotes the electric fields shift towards MBO region. The simulations are performed at the optimum mesh setting of the 'Hexahedral(legacy)' mesh type to keep a balance between the model accuracy and the model complexity, as shown in Fig. 2(a), where the chosen mesh configuration is denoted. The ε_r and simulated tunabilities variation, shown in Fig. 2(b), are discussed later in this Section. The average of overall bias fields at this mesh configuration, as shown in Fig. 2(c), are calculated to observe the division of bias fields between MBO and BST regions. Furthermore, the different random arrangements of BST and MBO cubes are influential in determining the average fields in the BST and the MBO region. Therefore, different random arrangements for each BST-MBO composition are simulated and the maximum deviation in the average bias fields in different regions is calculated, as shown with the shaded region in Fig. 2(c). The deviation of average bias fields in the BST region is not negligible but not influential in producing considerable deviation in the ε_r of the 50 vol-% BST composite varactor, as demonstrated by blue filled dots in Fig. 2(b). The deviation of 6% from the mean ε_r value is observed here, and the red triangle and the black square depict the extent of the maximum and the minimum ε_r possible. Hence, the model with mean of average field distribution in the BST region is chosen for further investigation for tunability studies. The bias electric field present in each BST mesh cell of this chosen model is then used to calculate the tuned ε_r of BST in that mesh cell, eventually, creating the complete tuned varactor model. Fig. 2(d) shows the bias fields Rayleigh parameter σ distribution across each mesh cell for various compositions of BST-MBO. The significance of this analysis is discussed later in this Section.

Based on Ginzburg–Landau theory, there are few ferroelectric tunability equations available — Vendik et al. [24], Chase et al. [25] and Weil et al. [26]. The Vendik et al. is heavily based on the physical material parameters, and is generally, used to understand the basic material properties. The Chase et al. is based on two parameters, which can easily be extract from measured data. The equation by Weil is located between these two equations, since it allows an improved adaptation to real measured data by using three parameters [27]. Therefore, Weil's equation is the optimum choice for this work which is given as

$$\varepsilon_r(E) = \varepsilon_r(0)\left[1 - \tau_\varepsilon(E_A)\frac{(1+a_1+a_2)\left|E/E_A\right|^2}{1+a_1\left|E/E_A\right|+a_2\left|E/E_A\right|^2}\right]. \tag{1}$$

Here a_1 and a_2 are the fitted parameters extracted from the electrical measurements of 100 vol-% BST varactor. E is the input bias electric field. Apart from these variable parameters, other parameters $\varepsilon_r(0)$, $\tau_\varepsilon(E_A)$ and E_A are the constants. $\varepsilon_r(0)$ is the maximum relative permittivity at $E = 0$ or zero DC bias, $\tau_\varepsilon(E_A)$ is the maximum tunability achieved at input bias electric field $E = E_A$. According to the 100 vol-% BST varactor data in Table 1, the $\tau_\varepsilon(E_A)$ is 41.2 % at E_A=1.1 kV/mm and under room temperature conditions around 24 °C which gives the fitting parameters a_1=4.364 and a_2=5.899. In observation, Eq. (1) fits well at both higher and lower bias in comparison with other equations. Using these extracted parameters and the bias electric fields extracted from CST Microwave Studio, the tuned ε_r is calculated for solids in each mesh cell in the BST region, individually, using Eq. (1). These tuned ε_r are then updated for the BST solids present at the respective mesh cells. An obtained color-coded tuned design model varactor for 80 vol-% BST is shown in the Fig. 3, where the more redness indicates the more tuned region i.e. more biased BST region. As an example, less bias field region (A) in the Fig. 1(e) shows the less tuned area in the Fig. 3 with black color and vice versa for the region (B) and (C). This tuned model varactor is then simulated to get the tuned capacitance. The tuned capacitance along with the untuned capacitance from the simulations, earlier, are used to calculate the overall tunability τ_C. The τ_C is equivalent to τ_ε for the parallel plate capacitors designed [21] and can be represented as

$$\tau_\varepsilon = \frac{C(0) - C(E)}{C(0)} = \frac{C(0) - C(\frac{V}{d})}{C(0)}, \tag{2}$$

where $C(0)$ and $C(E)$ are the capacitances at zero bias and at bias electric field E, respectively. V is the DC bias voltage applied across the capacitor and d is the capacitor's thickness. E is dependent on V and d, which makes the comparison of the distribution of bias fields in the designed varactor and the realized varactor equivalent. The V and d are scaled to maintain the same E. The dielectric loss study is neglected here as it is not the focus of this work.

In Fig. 2(d), the blue shaded region denotes the variation in σ values due to different random arrangements of BST and MBO in each composition. The σ values increase with increasing MBO content and then decrease again with MBO content increasing beyond 30 vol-%, as shown in Fig. 2(d). The reducing σ here denotes the shift of bias electric fields away from the BST region which is suspected to reduce tunabilities substantially. The calculated simulated tunabilities are shown in Fig. 4 with a blue triangled line. Upon observation, the tunabilities start declining rapidly around 70 vol-% MBO compositions which is in accordance with the shift of bias electric fields away from the BST region. This corresponds to the percolation threshold, as discussed in [16], where it happens around 67 vol-% MBO compositions. The percolation threshold in the simulated model varactor is also suspected to lie between 65 vol-% MBO composition and 70 vol-% MBO composition, as shown with the shaded red box in Fig. 2(d).

Table 1
Dielectric properties of the composite materials at room temperature (around 24 °C) at 13.56 MHz. The measured tunability is measured at 1.1 kV bias voltage. The simulated tunabilities for composites are calculated with fitting parameters from measurements of pure BST at room temperature. The lowered sintering temperatures and reducing dielectric loss in the mixtures of MBO and BST are the main benefits of the BST-MBO composite varactors. The notable degradation in tunabilities is also observed.

BST-MBO (in vol-%)	Sinter temperature (°C)	Meas. Q-factor Q_ε	Meas. τ_ε (%)	Simulated τ_ε (%)
100–0	1350	136	41.2	41.33
80–20	1050	205	7.8	40.11
70–30	1000	220	6	38.35
60–40	1000	286	5.9	37.72
50–50	1000	310	5.72	36.21
40–60	1000	340	4.75	35.12
30–70	1050	418	1.6	30.03
20–80	1100	850	0.72	17.52
10–90	1100	2714	0.025	4.09

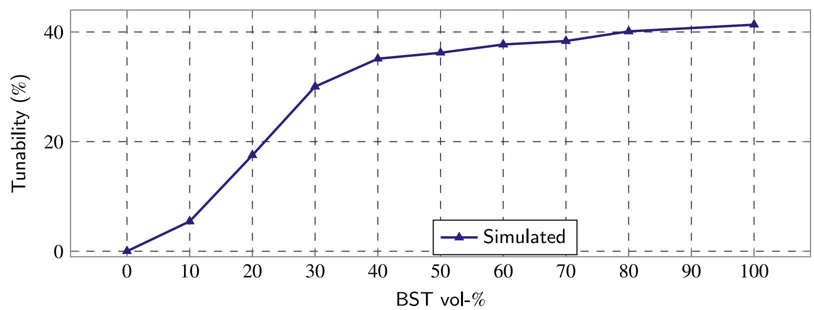

Fig. 4. Simulated tunability with 100 vol-% BST data at room temperature in blue triangles for different BST-MBO compositions.

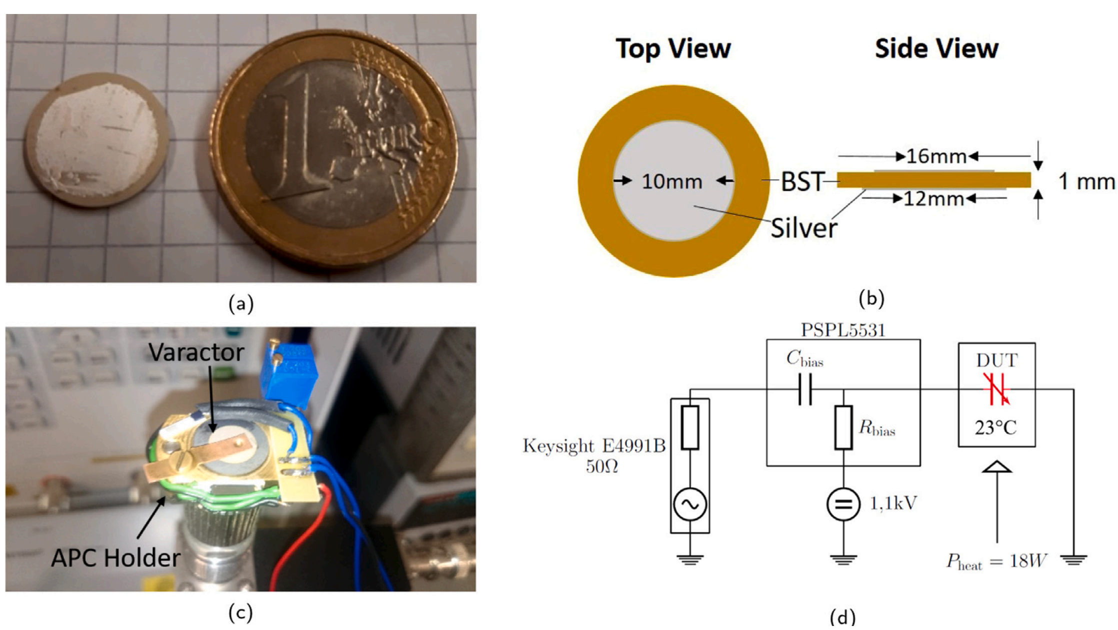

Fig. 5. Varactor pellets illustrations with (a) showing realized pellets, (b) displaying the pellets dimensions with top (left) and side (right) cut view, (c) depicting pellet holder and (d) demonstrating the schematic measurement circuit.

3. Fabrication, measurement and evaluation

3.1. Fabrication and experimentation

The MBO ($Mg_3B_2O_6$) is produced by mixing oxide process by using MgO and B_2O_3, and considering the required stoichiometric ratio. The mixed powder is grounded under aqueous conditions which is then calcined at 1200 °C for 2 h. However, the BST ($Ba_{0.6}Sr_{0.4}TiO_3$) is synthesized by the sol–gel approach, using barium acetate, strontium acetate and titanium isopropoxide. The thoroughly mixed sol in the aqueous condition is then calcined at 1100 °C for 2 h. The prepared BST is then milled to desired particle size to increase sinter activity, and then, mixed with MBO to produce different vol-% of BST and MBO composite varactors. The different granulated powder mixtures are pressed under 150 MPa using a single-axis manual press to form solid pellets. These pellets are then sintered at different temperatures to densify the pellets. The decrease of sintering temperature of the composite pellets from the pure BST pellet shows another benefit of using BST-MBO composites. Finally, the sintered pellets are metalized for the electrical and temperature characterization. The resultant pellets are shown in Fig. 5(a) and the probable dimensions are shown in Fig. 5(b). Table 1

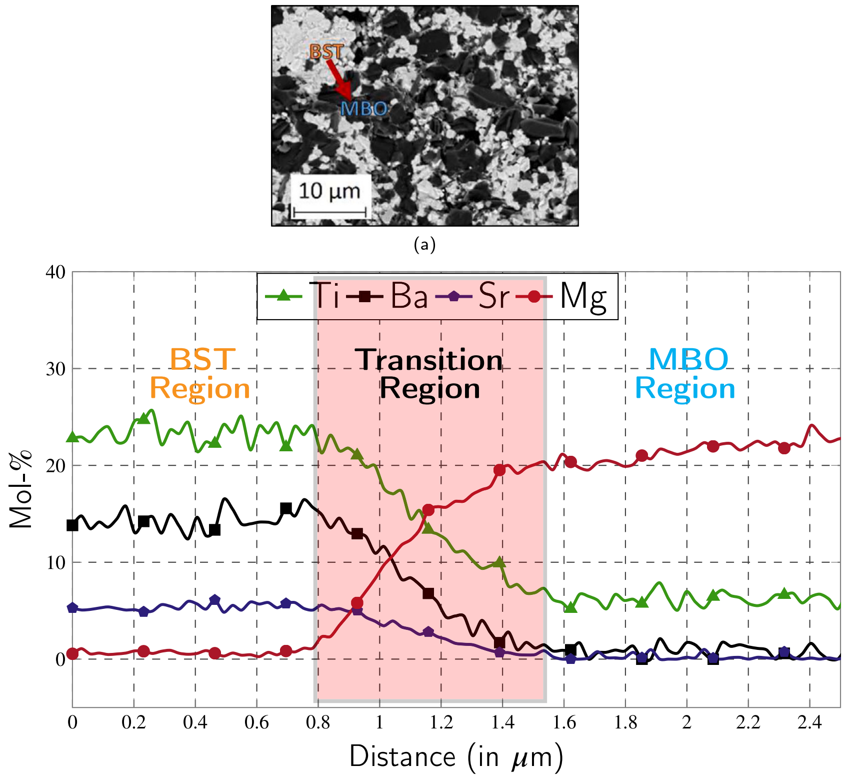

(a)

(b)

Fig. 6. (a) depicts the SEM image of the 40 vol − % BST pellet with BST in white color and MBO in black color. The red line denotes the path of the EDX line scan as shown in (b) for the 40 vol − % BST pellet. The undesirable detection of Ti^{4+} ions in MBO region, shown by the green filled triangle line in (b), denotes the substitution effect. This substitution effect leads to the formation of third phase and the presence of this third phase is witnessed in SEM image with gray color and is suspected to be Mg_2TiO_4 [28]. (For interpretation of the references to color in this figure legend, the reader is referred to the web version of this article.)

Table 2
Measured Curie temperature T_C and extracted input fitting parameters for updated electrical characterization for different BST-MBO vol-% composite varactors.

BST-MBO (in vol-%)	T_C (°C)	100 vol-% BST varactor		
		$T_{M,updated}$ (°C)	$\tau_{\varepsilon,updated}$ (%)	Fit parameters (a1,a2)
100–0	3	24	41.2	(4.364, 5.899)
80–20	−20	47	9.35	(−0.1342, 0.2767)
70–30	−19	46	9.35	(−0.1342, 0.2767)
60–40	−22	49	7.5	(−1.272, 0.6316)
50–50	−24	51	7.25	(4748, −1934)
40–60	−29	56	6.2	(4.168, −2.503)

demonstrates the different BST-MBO composite varactors, ranging from 10 to 100 vol-% BST, considered in this work.

3.2. Initial electrical characterization

Electrical characterization of the bulk ceramic disk varactor samples is performed in a temperature-controlled pellet holder, see Fig. 5(c). The pellet holder is based on APC-7 standard and establishes a connection to the top and bottom electrode of the pellet. The maximum temperature of up to 70 °C can be achieved in this setup. Small-signal analysis is performed around 13.56 MHz with a Keysight Impedance Analyser E4991B using the DC bias source Keithley 2410. The schematic measurement circuit is shown in Fig. 5(d). The impedance analyzer monitors the extracted capacitance and Q-factor over biasing voltages from 0 V up to 1100 V with 100 V step size and at room temperature. Before every measurement, the setup is calibrated by standard short, open and load (SOL) calibration at the end of the bias circuit with the DC bias source switched on at 0 V.

Initially, the 100 vol-% BST varactor is measured to extract the input parameters for Eq. (1) of capacitance tunability, discussed in Section 2. Using curve fitting, parameters a_1 and a_2 are extracted from the 100 vol-% BST, as mentioned in Table 2. The varactor model uses this information to simulate for all the volumetric compositions of BST and MBO mentioned in Table 1. For the same volumetric composition, the electrical measurements are also recorded to compute the tunability τ_ε and Q-factor Q_ε variations. The gradual increase of Q_ε and decrease of sinter temperature exemplify the viability of the mixtures of BST and MBO. However, a notable discrepancy is observed in the values of measured and simulated tunabilities, at all the compositions. For 80 vol-% BST composition, around 33% drop in measured tunability is witnessed, in comparison, with the simulated results.

3.3. Substitution effect

According to Tagantsev et al. [18], the electric properties are governed mainly by two factors — composite and doping effects. The composite effects are visible in the simulation results as well as in the measurements for all the composite varactors. But doping effects are not incorporated in the simulations. Generally, the doping effect is defined, primarily, for the reduction of capacitance tunability in

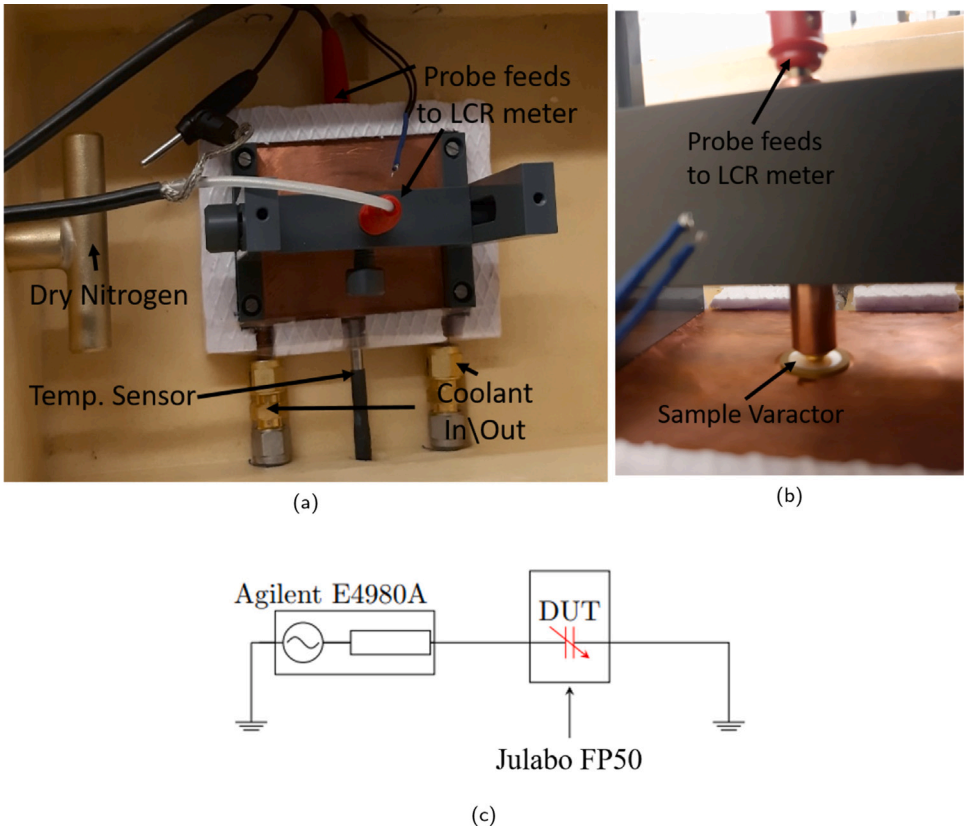

Fig. 7. Temperature measurement setup for measuring Curie temperatures T_C between −30 °C and 30 °C with top view in (a), side view in (b) and schematic circuit diagram in (c).

the doping concentrations but here it is observed that this effect is not limited to doping concentrations as the tunability decreases at a higher rate in measurements with more than 20 vol-% MBO. For this reason, the doping effect is referred to as the substitution effect in this work. Chemically, the substitution effect represents the ionic exchanges between the BST and MBO. For a better understanding of the occurring substitution, a microstructure study is conducted using a scanning electron microscope (SEM) (Supra 55, Zeiss, Oberkochen) which is equipped with an EDX setup (EDAX, AMETEK GmbH, Wiesbaden) to observe the elemental metal distribution in the composite varactor under test. The captured SEM image is shown in Fig. 6(b) for 40 vol − % BST varactor. The EDX line scan is recorded for the same composite varactor, as shown in Fig. 6(a), which shows the elemental distribution across the BST and MBO regions. In the BST region, no recognizable substitution is observed, particularly, the Mg^{+} substitution, which has been suggested in [16]. Although, weak Mg^{+} doping might be suppressed under the detection limit of the EDX. However, in the MBO region, a considerable amount of Ti^{4+} ions diffusion from the BST region is witnessed. This leads to significant oxygen vacancies in the BST region. Since, the central position in the BST lattice is either unoccupied or substituted by another element, affects the tunabilities severely. Additionally, the image analysis of SEM recordings of the 40 vol − % BST varactor illustrates the presence of third phase in gray color apart from BST (white) and MBO (black), as shown in the Fig. 6(b). Apart from these, XRD analysis is performed which is mentioned in [28]. According to this, the third phase is suspected to be Mg_2TiO_4, although, the amount detected is too little to consider.

3.4. Updated electrical characterization

The substitution effect directly affects the Curie temperature (T_C) of the composites, as has been observed in [29], which makes it crucial to include the substitution effect in the simulation varactor model. Therefore, a detailed thermal characterization is done between −30 °C and 30 °C for composite varactors acknowledging that the 100 vol-% BST varactor has a theoretical T_C of around 2 °C [23]. The capacitance readings are recorded using Agilent E4980 A LCR meter at 1 MHz, as the T_C is independent of frequency and the readings are valid for the working radio frequency as well. The manufactured setup for these measurements is shown in Fig. 7. The top view, side view and schematic circuit of this setup are shown in Figs. 7(a)–7(c), respectively. Here temperature-controlled liquid from Julabo FP50 cooling unit is made to flow in the metal block, over which varactor is placed and temperature close to the varactor is measured by a Pt100 temperature sensor. The measured temperature is taken as feedback to control the temperature out of the cooling unit. This process is repeated until the desired temperature is achieved. After reaching the desired temperature, the capacitance measurements are taken. In addition, dry nitrogen is made to flow in the vicinity of the varactor, to prevent the frosting and defrosting effects due to the temperature variations. The temperature at which the highest capacitance is achieved is the T_C of that varactor. The T_C is measured for varactor with BST composition of 100, 80, 70, 60, 50 and 40 vol-%, which is shown in Table 2. Due to the limitations of the temperature range achieved, the T_C could not be measured for other varactor compositions. The 100 vol-% BST varactor is having T_C of around 3 °C which is quite near to the theoretical BST's T_C of around 2 °C [23]. Comparing with the 80 vol-% BST varactor, which has −20 °C of T_C, there was around 23 °C shift in T_C. The shift in T_C and decline in capacitance tunability is seen in all the composite varactors measured and is observed that it is proportional to the substitution effect.

The T_C shifts cannot be ignored and a solution to compensate the gap is needed for the varactor model to simulate real scenario results, as T_C shift is, prominently, a material effect than an electrical effect to include in the CST simulation environment. To incorporate the effect of

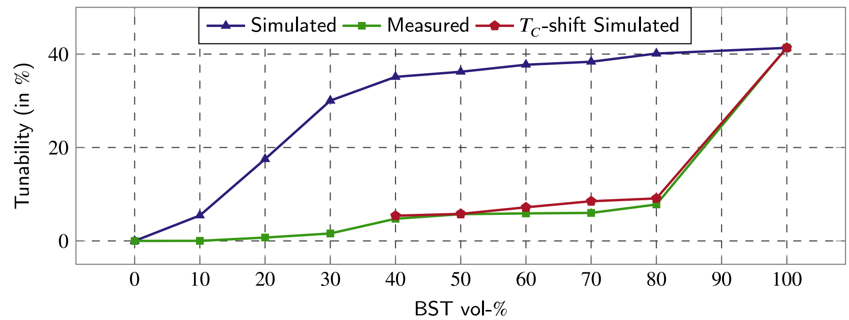

Fig. 8. Tunability comparison between simulations with 100 vol-% BST varactor data at room temperature in blue triangles, measurements in green squares and T_C-shifted simulations with 100 vol-% BST varactor data at different temperatures in red pentagons. All the measured observations shown, are performed at 13.56 MHz under room temperature conditions and 1100 V maximum bias.

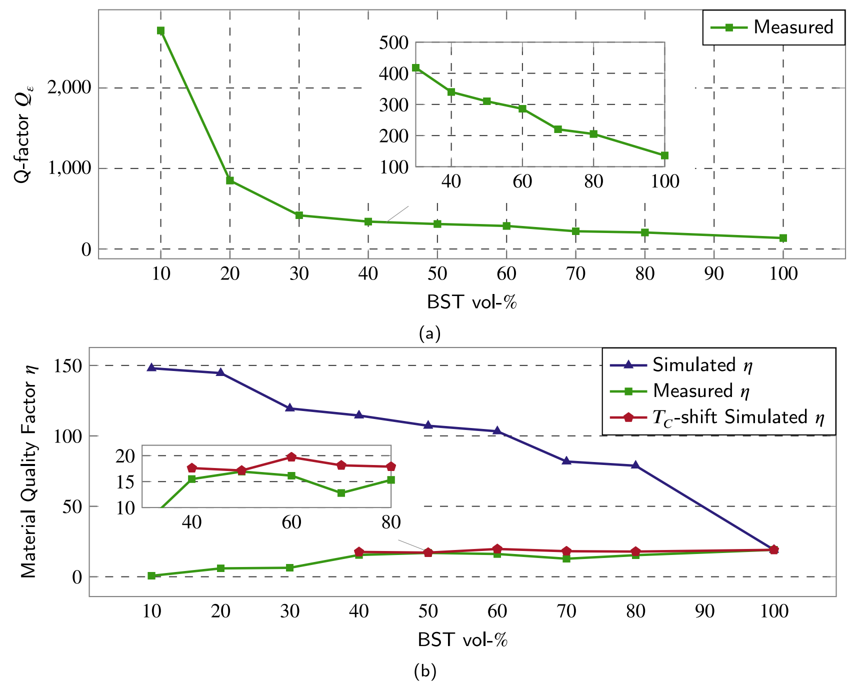

Fig. 9. (a) demonstrates the measured untuned Q-factor Q_ε of untuned BST-MBO composite varactor at 13.56 MHz under room temperature. (b) depicts the material quality factor η comparisons between simulations, measurements and T_C-shifted simulations.

T_C shift, the 100 vol-% BST is measured at $T_{M,updated}$, which is shifted by the gap between the T_C of 100 vol-% BST and composite varactors.

$$T_{M,updated} = T_M + [T_C(100) - T_C(y)], \quad (3)$$

where $T_{M,updated}$ is the updated measured temperature of 100 vol-% BST, T_M is regular measure temperature i.e. room temperature around 24 °C and $T_C(y)$ is the T_C of y vol-% BST composite varactor. The result of this 100 vol-% BST varactor's measurement at the updated temperature is considered for the inputs in Eq. (1) in the Section 2, for updating the simulation varactor model. The calculated $T_{M,updated}$ for the different compositions is given in Table 2. For 80 vol-% and 70 vol-% BST composite varactor, the measurements of 100 vol-% BST varactor measured at 46-47 °C is considered for parameter extraction for Eq. (1) as the difference in T_C is negligible. Similarly, for 60, 50 and 40 BST vol-% compositions in consideration, the measurements of 100 vol-% BST varactor measured at 49 °C, 51 °C and 56 °C, respectively, are considered for parameter extraction. After simulating the T_C shift-adjusted tuned varactor model for all compositions, the calculated simulated tunabilities are observed close to measured tunabilities as shown in Fig. 8. For all compositions, the difference in tunabilities is reduced from around 32% to under 2.5%. The measured tunabilities are still slightly deviated from simulated tunabilities which is due to the lack of consideration of real shapes of each material's phase in the model. In addition, the cubical shapes of each phase are responsible for corner radiation effects, leading to a slight increase in the tuning of BST at the corner interface of BST and MBO. However, slight thermal vulnerabilities in the high-temperature measurements of the 100 vol-% BST varactor are also observed to be the reason for the deviation as it effects the results from Eq. (1). The untuned Q_ε is illustrated in Fig. 9(a), showing the increasing Q_ε with increase in MBO vol-%. The figure-of-merit is considered as the material quality factor η [30], defined as

$$\eta = Q_\varepsilon \cdot \tau_\varepsilon, \quad (4)$$

as shown in Fig. 9(b) for all composite varactors. The Q_ε is considered the same as in Fig. 9(a) for all simulations and measurements but the tunabilities are taken from Fig. 8 for the respective simulations and measurements. The varactor with 50 vol-% BST illustrates the most optimum performance with η around 18, although, the τ_ε is less than the higher BST content varactor. This trade-off between Q_ε and τ_ε is crucial for low-loss varactors. Moreover, these composite varactors are expected to operate till at least 4 kV, which will further increase the η, substantially [31].

4. Conclusion and outlook

The presented work demonstrates a study of tunable ferroelectric and dielectric composite materials with high contrast in relative permittivity. The experimental analysis demonstrates the viability of composites with an increase in the Q_{ϵ} with MBO addition, which is important for low-loss varactors. However, this is achieved at the cost of a huge reduction in tunability. Therefore, an electromagnetic model to determine the tunability over a full range of volume compositions is proposed based on the distribution of bias electric fields. A composite material consisting of $Mg_3B_2O_6$ (MBO) as dielectric and $Ba_{0.6}Sr_{0.4}TiO_3$ (BST) as tunable ferroelectric is fabricated for various compositions and characterized at room temperature and 13.56 MHz. The results show that the electric field distribution approach effectively predicts the tunable properties over the entire mixing range. Since, it deviates heavily from the measured dielectric properties and additional degrees-of-freedom are required to consider the material changes with the mixing. With the microstructure studies, it is illustrated that the leakage of Ti^{4+} into the MBO region is responsible for this huge deviation in tunability, which is defined as the substitution effect in this work. This substitution effect is directly related to T_C shifts in the composite varactor. A solution is devised in this work to incorporate the T_C shifts in the model and, after implementation, it is shown that T_C-shifted model predicted simulated results are close to the measured results. According to the author's knowledge, this is the first model effectively predicting the tunabilities, which are in agreement with the measured tunabilities. To effectively prove the efficiency of the model, efforts will be made by mixing other dielectric additives in the future.

CRediT authorship contribution statement

Prannoy Agrawal: Conceptualization, Methodology, Software, Data curation, Writing – original draft. **Stipo Matic:** Writing – review & editing. **Kevin Häuser:** Material fabrication, Writing – review & editing. **Joachim R. Binder:** Writing – review & editing, Funding acquisition. **Holger Maune:** Writing – review & editing. **Ersin Polat:** Writing – review & editing. **Rolf Jakoby:** Supervision, Writing – review & editing, Funding acquisition.

Declaration of competing interest

The authors declare that they have no known competing financial interests or personal relationships that could have appeared to influence the work reported in this paper.

Acknowledgments

The authors would like to acknowledge the funded support from Deutsche Forgemeineschaft (DFG) under the project BI 1636/2-3 and JA 921/37-3. Apart from this, special thanks for external support from Comet AG (Flamatt, Switzerland) to the project.

References

[1] F. Fang, Towards atomic and close-to-atomic scale manufacturing, Int. J. Extrem. Manuf. 1 (2012) 012001.

[2] K.J. Kanarik, S. Tan, R.A. Gottscho, Atomic layer etching: Rethinking the art of etch, Int. J. Phys. Chem. Lett. 9 (16) (2018) 4814–4821.

[3] Y. Chen, Tunable Decoupling and Matching Concepts for Compact Mobile Terminal Antennas (PhD dissertation), Gottfried Wilhelm Leibniz Universität Hannover, Hannover, Germany, 2017.

[4] C.M. Andersson, N. Ejebjork, A. Henry, S. Andersson, E. Janzen, H. Zirath, N. Rorsman, A SiC varactor with large effective tuning range for microwave power applications, IEEE Electron Device Lett. 32 (6) (2011) 788–790.

[5] R.H. Caverly, PIN diode switching speed for MRI applications, in: IEEE MTT-S International Microwave Biomedical Conference, IMBioC, Toulouse, France, 2020, pp. 1–3.

[6] R.D. Streeter, C.A. Hall, R. Wood, R. Mahadevan, VHF high-power tunable RF bandpass filter using microelectromechanical (MEM) microrelays, Int. J. RF Microw. Comput.-Aided Eng. 11 (5) (2001) 261–275.

[7] L.-Y. Ma, N. Soin, M.H. Mohd Daut, S.F. Wan Muhamad Hatta, Comprehensive study on RF-MEMS switches used for 5G scenario, IEEE Access 7 (2019) 107506-107522.

[8] D. Kienemund, N. Bohn, T. Fink, M. Abrecht, W. Bigler, J.R. Binder, R. Jakoby, H. Maune, Acoustical behavior of fully-printed, BST mim varactor modules in high power matching circuits, in: IEEE/MTT-S International Microwave Symposium, IMS, Philadelphia, USA, 2018, pp. 1393–1396.

[9] X. Wang, F. Xia, N. Li, J. Wang, C. Li, X. Zhang, Y. Bian, G. Li, Y. Wu, H. Li, L. Sun, Y. He, A YBCO/BST/MgO interdigital varactor and an L-band tunable HTS bandpass filter, in: Advanced Materials and Processes for RF and THz Applications, IMWS-AMP, Suzhou, China, 2015, pp. 1–3.

[10] K. Annam, D. Spatz, E. Shin, G. Subramanyam, Experimental verification of microwave phase shifters using barium strontium titanate (BST) varactors, in: IEEE National Aerospace and Electronics Conference, NAECON, Ohio, USA, 2019, pp. 63–66.

[11] D. Mercier, A. Niembro-Martin, H. Sibuet, C. Baret, J. Chautagnat, C. Dieppedale, C. Bonnard, J. Guillaume, G.Le. Rhun, C. Billard, et al., X band distributed phase shifter based on sol–gel BCTZ varactors, in: Proceedings of the IEEE 2017 European Radar Conference, EURAD, Nuremberg, Germany 11–13, 2017, pp. 382–385.

[12] Q. Zhang, L. Wang, J. Luo, Q. Tang, J. Du, $Ba_{0.4}Sr_{0.6}TiO_3$/MgO composites with enhanced energy storage density and low dielectric loss for solid-state pulse-forming line, Int. J. Appl. Ceram. Technol. 7 (2009) E124–E128.

[13] Y.H. Huang, J.W. Yong, Q. Weijian, L. Juan, M.C. Xiang, Enhanced energy storage density of $Ba_{0.4}Sr_{0.6}TiO_3$–MgO composite prepared by spark plasma sintering, J. Eur. Ceram. Soc. 35 (2015) 1469–1476.

[14] L. Tang, Y. Bian, J. Zhai, H. Zhang, Ferroelectric-dielectric composites model of $Ba_{0.5}Sr_{0.5}TiO_3/Mg_2AO_4$(A = Ti, Si) for tunable application, J. Am. Ceram. Soc. 97 (3) (2014) 862–867.

[15] X. Chou, J. Zhai, X. Yao, Dielectric tunable properties of low dielectric constant Ba0.5Sr0.5TiO3–Mg2TiO4 microwave composite ceramics, Appl. Phys. Lett. 91 (12) (2007) 122908.

[16] Q. Zhang, J. Zhai, X. Yao, Dielectric and percolative properties of $Ba_{0.5}Sr_{0.5}TiO_3$-$Mg_3B_2O_6$ composite ceramics, J. Am. Ceram. Soc. 94 (4) (2011) 1138–1142.

[17] L. Jylha, A. Sihvola, Tunability of granular ferroelectric dielectric composites, Electromagn. Waves (Camb) 78 (2008) 189–207.

[18] A.K. Tagantsev, V.O. Sherman, K.F. Astafiev, J. Venkatesh, N. Setter, Ferroelectric materials for microwave tunable applications, J. Electroceramics 11 (1) (2003) 5–66.

[19] V.O. Sherman, A.K. Tagantsev, N. Setter, D. Iddles, T. Price, Ferroelectric-dielectric tunable composites, J. Appl. Phys. 99 (7) (2006) 074104.

[20] M. Lei, The impact of composite effect on dielectric constant and tunability in ferroelectric–dielectric system, J. Am. Ceram. Soc. 98 (10) (2015) 3250–3258.

[21] A. Wiens, C. Kohler, M. Hansli, M. Schuessler, M. Jost, H. Maune, J.R. Binder, R. Jakoby, CAD-Assisted modeling of high dielectric contrast composite materials, J. Eur. Ceram. Soc. 37 (4) (2017) 1487–1494.

[22] X. Ma, S. Li, Y. He, T. Liu, Y. Xu, The abnormal increase of tunability in ferroelectric-dielectric composite ceramics and its origin, J. Alloys Compd. 739 (2018) 755–763.

[23] J.H. Jeon, Effect of SrTiO3 concentration and sintering temperature on microstructure and dielectric constant of Ba1-xSrxTiO3, J. Eur. Ceram. Soc. 24 (6) (2004) 1045–1048.

[24] O.G. Vendik, S.P. Zubko, Modeling the dielectric response of incipient ferroelectrics, J. Appl. Phys. 82 (9) (1997) 4475–4483.

[25] D.R. Chase, L. Chen, R.A. York, Modeling the capacitive nonlinearity in thin-film BST varactors, IEEE Trans. Microw. Theory Techn. 53 (10) (2005) 3215–3220.

[26] C. Weil, Passiv Steuerbare Mikrowellenphasenschieber Auf Der Basis Nichtlinearer Dielektrika (Ph.D. Dissertation), Technical University of Darmstadt, Darmstadt, Germany, 2003.

[27] H. Maune, Design Und Optimierung Hochlinearer Ferroelektrischer Varaktoren Für Steuerbare Hochfrequenz-Leistungsverstärker (Ph.D. Dissertation), Technical University of Darmstadt, Darmstadt, Germany, 2011.

[28] K. Häuser, R. Azmi, P. Agrawal, R. Jakoby, H. Maune, M.J. Hoffmann, J.R. Binder, Sintering behavior and electrical properties of the paraelectric/dielectric composite system BST/MBO, J. Eur. Ceram. Soc. 41 (14) (2021) 7022–7028.

[29] B. Su, T.W. Button, Microstructure and dielectric properties of Mg-doped barium strontium titanate ceramics, J. Appl. Phys. 95 (3) (2004) 1382–1385.

[30] A. Giere, Material- Und Bauteiloptimierung Steuerbarer Mikrowellenkomponenten Mit Nichtlinearen Ferroelektrika (Ph.D. Dissertation), Technical University of Darmstadt, Darmstadt, Germany, 2009.

[31] P. Agrawal, D. Kienemund, D. Walk, S. Matic, N. Bohn, K. Häuser, T. Fink, M. Abrecht, W. Bigler, J.R. Binder, R. Jakoby, H. Maune, Suppression of acoustic resonances in BST-based bulk-ceramic varactors by addition of magnesium borate, Crystals 11 (7) (2021) 786.

Prannoy Agrawal *Institute for Microwave Engineering and Photonics, Technical University of Darmstadt, Darmstadt, Germany*. Prannoy Agrawal was born in New Delhi, India, in 1991. He received the bachelor's degree from GGSIP University, New Delhi, in 2012, and the master's degree from the Technische Universität Darmstadt, Darmstadt, Germany, in 2018. Since 2018, he has been with the Institute of Microwave Engineering and Photonics, Technische Universität Darmstadt. His current research interests include tunability and acoustic resonances modeling of barium strontium titanate (BST) composites and high-power varactors.

Stipo Matic *Institute for Microwave Engineering and Photonics, Technical University of Darmstadt, Darmstadt, Germany*. Stipo Matic was born in Wiesbaden, Germany, in 1991. He received the B.Sc. and M.Sc. degrees from Technische Universität Darmstadt, Darmstadt, Germany, in 2017 and 2020, respectively, where he is currently pursuing the Ph.D. degree at the Institute for Microwave Engineering and Photonics. His current research interests include the design and integration of reconfigurable components based on the ferroelectric material barium strontium titanate.

Kevin Häuser *Institute of Applied Materials, Karlsruhe Institute of Technology, Karlsruhe, Germany*. Kevin Häuser studied physics in Heidelberg and Uppsala University with a focus on solid state physics, material science and microelectronics. After his studies, he was a Ph.D. student at Karlsruhe Institute of Technology from 2017 until 2021, working on composite ceramic materials and structural effects on electronic properties of capacitors. He is currently employed at the Robert Bosch GmbH, where he is developing MEMS sensors for automotive applications.

Joachim R. Binder *Institute of Applied Materials, Karlsruhe Institute of Technology, Karlsruhe, Germany*. Joachim R. Binder received the diploma degree in chemistry and the Ph.D. degree from the University of Osnabrück, Germany, in 1993 and 1997, respectively. In 1997, he joined the Karlsruhe Institute of Technology (former Forschungszentrum Karlsruhe), Germany, where he has been a group leader at the Institute of Applied Materials (IAM-ESS) since 1999. His current research is dedicated to material and process development, especially tailored composites for tunable microwave dielectrics, inks for the printed electronics as well as the material design of lithium ion and of post lithium battery materials.

Holger Maune *Microwave and Communication Engineering, Otto von Guericke University Magdeburg, Magdeburg, Germany*. Holger Maune was born in Cologne, Germany, in 1981. He received the Dipl.-Ing., Dr.-Ing., and the venia legend degree in communications engineering from the Technische Universität Darmstadt, Darmstadt, Germany, in 2006, 2011 and 2020, respectively. He has been Full Professor of electrical engineering and holds the Chair of Microwave and Communication Engineering at the University of Magdeburg, Germany since 2021. His research is currently focused on advanced RF devices employing tunable dielectrics for adaptive/reconfigurable systems, and for high power applications.

Ersin Polat *Institute for Microwave Engineering and Photonics, Technical University of Darmstadt, Darmstadt, Germany*. Ersin Polat was born in Alzenau, Germany, in 1991. He received the B.Sc. and M.Sc. degrees in electrical engineering and information theory from Technische Universität Darmstadt, Darmstadt, Germany, in 2014 and 2017, respectively, where he is currently pursuing the Ph.D. degree with the Microwave Engineering Group. He currently leads the Tunable Radio Frequency Devices research group at the institute of microwave engineering and photonics, TU Darmstadt. His current research interests include tunable microwave filters based on liquid crystal technology and material characterization.

Rolf Jakoby *Institute for Microwave Engineering and Photonics, Technical University of Darmstadt, Darmstadt, Germany*. Rolf Jakoby was born in Kinheim, Germany, in 1958. He received the Dipl.-Ing. and Dr.-Ing. degrees in electrical engineering from the University of Siegen, Germany, in 1985 and 1990, respectively. In 1991, he joined the Research Center of Deutsche Telekom in Darmstadt, Germany. Since 1997 he has been a Full Professor for Microwave Engineering at Technische Universität Darmstadt, Germany. He is a co-founder of ALCAN Systems GmbH, a smart antenna company. Rolf Jakoby is author of more than 599 publications (161 in journals) and holds more than 23 patents. His current research interests include chipless RFID sensor tags, biomedical sensors and applicators as well as tunable passive microwave devices and beamsteering antennas, using electromagnetic bandgap structures, ferroelectric and liquid crystal technologies. He received an award from CCI Siegen for his excellent Ph.D. in 1992 and the ITG-Prize in 1997 for an excellent publication in the IEEE AP Transactions. His group received 24 awards and prizes for best papers and doctoral dissertations. He is editor-in-chief of FREQUENZ, DeGruyter, member of VDE/ITG and of IEEE/MTT/AP societies. He was Chairman of the EuMC in 2007 and GeMiC in 2011 and was Treasurer of the EuMW in 2013 and 2017, respectively.